Journal of Electrical Engineering & Technology (2020) 15:1155–1165
https://doi.org/10.1007/s42835-020-00418-5

ORIGINAL ARTICLE

Mitigating Disturbance in Harmonic Voltage Using Grid-side Current Feedback for Grid-connected LCL-filtered Inverter

Ye Zhang[1] · Muqin Tian[1] · Jiancheng Song[1] · Xiaoyu Zhang[1]

Received: 30 August 2019 / Revised: 6 January 2020 / Accepted: 26 March 2020 / Published online: 7 April 2020

Abstract
As the interface between new energy and power grid, the grid-connected LCL-filtered inverter plays a key role in energy conversion. However, it performs poor at rejecting grid background harmonics that distort the grid-side current and affect the quality of the output power of the inverter. Thus, a feedback strategy for the grid-side current employing the proportional integral and resonant controller (PI + HC) is used to mitigate the harmonics of the grid-side current and improves the quality of the output power of the grid-connected LCL-filtered inverter. Owing to the grid-side current feedback control system is unstable, improved High Pass Filter (HPF) active damping based on unit delay feedback is used to guarantee stability and effectiveness of PI + HC. The proposed method for mitigating grid-side current harmonics is validated by a detailed simulation and the results of experiments.

Keywords Grid-connected LCL-filtered inverter · Grid background harmonics · Grid-side current feedback · PI + HC · Improved HPF

1 Introduction

With the development of new energy technology, grid-connected inverters have received considerable research attention [1]. However, the output current of the inverter contains a large number of switching frequency harmonics, because of which an L-type or LCL-type filter needs to be added between the inverter and the grid to satisfy the requirements of grid connection. Compared with the L-type filter, the LCL-type filter is used more commonly owing to its small volume, low cost and strong attenuation of high-frequency switching ripples [2–4]. However, the LCL-type filter suffers from resonance problem, so effective damping becomes necessary to ensure the stability of the system. Two methods, including passive damping and active damping, are employed to damp the resonance of LCL-type filter [5–11]. Compared with passive damping solutions, active damping methods are more efficient and flexible, and thus are more commonly used [12–17]. It is usually realized by current loop control and this paper chooses grid-side current feedback for its simplicity.

In addition to the LCL-type filter resonance, the grid background harmonics caused by nonlinear loads can distort the grid-side current and degrade the quality of the output power of the inverter, which makes the grid-side current difficult to meet the grid standards, such as IEEE 519-1992 and IEEE 929-1988.

Many researches have been done to suppress the negative effects on the grid connected LCL-filtered inverter of grid background harmonics [18–28]. The methods to mitigate distortion of the output current are mainly divided into inverter-side current feedback control, grid-side current feedback control.

Inverter-side current feedback was used to suppress the distortion of the output current caused by grid background harmonics [18–20]. However, this strategy failed to obtain the harmonic information because the harmonic currents flew through the filter capacitor. The current/voltage of the partial capacitor, or grid voltage needs to be sampled to acquire the harmonic information of the grid-side current, which increases invest cost and system complexity.

The grid-side current feedback is an effective strategy to suppress the distortion of the output current [19, 21–28]. Twining and Holmes proposed a dual loop control strategy

✉ Muqin Tian
Tianmuqin@163.com

[1] Taiyuan University of Technology, Taiyuan, China

with the grid current outer loop using proportional-integral controller and the inner capacitance current loop using proportional controller [21]. But the authors did not point out the physical significance of the inner controller. Liu et al. [22] gave a parameter design process of the dual loop controller using pole placement and pole-zero cancellation, but it was too difficult to calculate and realize based on the work of Twining and Holmes [21]. A dual-sequence adaptive-gain variable-structure voltage control scheme was applied for effective mitigation of random and aperiodic grid disturbances [19]. However, this method required designing an appropriate sliding surface. Furthermore, the sliding-mode control exhibited jitter problem. A capacitor-current-feedback active damping and a proportional resonant regulator with harmonic compensation were adopted to achieve strong robustness of stability and high harmonic-rejection ability [23, 24]. When many kinds of harmonics need to be suppressed, it is necessary to design more resonance controllers, which will increase complexity of the control and degrade stability of the system. Using a double closed-loop control strategy based on inductor voltage difference and grid current feedback [25], can suppress the grid background harmonics effectively. However, inductor voltage difference will amplify the effect of noise and is difficult to be implemented in the experimental system. A feedforward scheme based on the band-pass-filter (BPF) was used to compensate the grid harmonics at the selected frequencies [26]. To realize high rejection of grid current low-order harmonics, the band-pass filters at the harmonic frequencies were used to detect the variation of the grid impedance as well as to facilitate the adaptive PCC voltage feedforward [27]. A Kalman filter was used by employing output current and grid voltage to remove the effect of grid voltage disturbances on the output current [28]. This method depends on the accurate model of the plant. Unified Power Quality Controller (UPQC) was utilized to compensate voltage and current distortions simultaneously in multi-feeder system [29].

The grid-side current feedback methods mentioned above used active damping with feedback of capacitor current, capacitor voltage, inductor voltage or feedforward of grid voltage to ensure stability of the control system. In this way, additional sensors are required to sample the capacitance current, capacitance voltage, inductor voltage and grid side voltage, which will increase the hardware cost.

This paper investigates the impact of the grid background harmonics on the output current of grid-connected LCL filtered inverter from the perspective of grid impedance. PI + HC is used to suppress the harmonics of the grid-side current in *dq* synchronous frame which can reduce complexity of the control system with fewer resonant controllers. However, the single-loop grid-side current feedback control system suffers from stability problem, so improved HPF is proposed by employing the grid-side current. The proposed method can suppress the distortion of the output current effectively and reduce hardware invest compared with other active damping.

The remainder of this paper is organized as follows: Section 2 presents the grid-connected LCL-filtered inverter with PI + HC and analyzes stability of the grid-side current feedback control system. Section 3 is devoted to designing an improved HPF and choosing the optimized feedback coefficient. Section 4 presents the results of simulation and experiments. Finally, Sect. 5 gives the conclusions of this study.

2 System Model and Stability Analysis of GCF

Figure 1 shows the topology of a three-phase grid-connected LCL-filtered inverter with the GCF control strategy, where the filter consists of an inverter inductor L_1, capacitor C and grid inductor L_2.

The derivative resistances of the inductors are negligible to denote the most extreme case. The inverter is supplied with input DC voltage V_{dc}, while v_{gf} and v_{gh} represent the grid voltage and grid background harmonics, respectively. i_2^* is the reference of the grid-side current.

2.1 Current Controller Based on PI + HC

The grid background harmonics arise from the nonlinear load connected in the power grid, which will affect the waveform quality of the grid-side current.

The equivalent block diagram of the grid-side current feedback control is shown in Fig. 2.

According to Fig. 2, the grid-side current i_2 can be calculated from the reference current i_2^* and the grid voltage v_g based on (1):

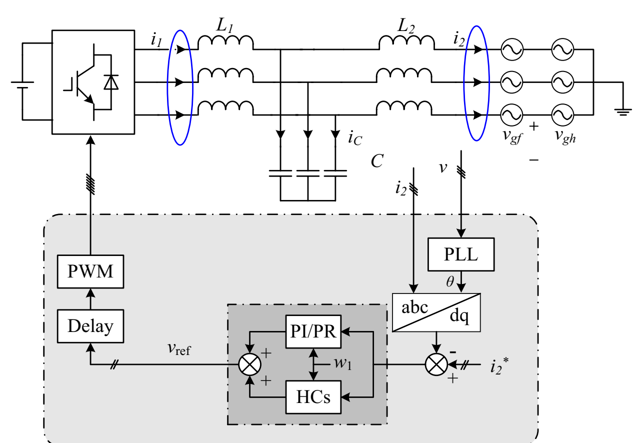

Fig. 1 Topology of three-phase grid-connected LCL-filtered inverter with GCF

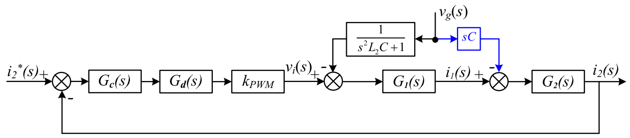

Fig. 2 Equivalent block diagram of the grid-side current feedback control

$$i_2 = \frac{G_c(s)G_d(s)G_1(s)G_2(s)}{1 + G_c(s)G_d(s)G_1(s)} i_2^* - \left(\frac{G_1(s)G_2^2(s)}{1 + G_c(s)G_d(s)G_1(s)} + sCG_2(s) \right) v_g \tag{1}$$

where $G_c(s)$ represents the current controller, $G_d(s) = e^{-1.5sT_s}$, $G_1(s) = \frac{s^2L_2C+1}{s^3L_1L_2C+s(L_1+L_2)}$, $G_2(s) = \frac{1}{s^2L_2C+1}$ and $\omega_{res} = \sqrt{(L_1+L_2)/L_1L_2C}$.

Then (1) can be transformed to (2):

$$i_2 = \frac{T(s)G_2(s)}{1 + T(s)} i_2^* - \frac{G_1(s)G_2^2(s) + sCG_2(s)T(s)}{1 + T(s)} v_g \tag{2}$$

where $T(s) = G_c(s)G_d(s)G_1(s)$, $G_c(s) = G_{PI}(s) + G_R(s)$.

It can be seen from (2) that when $T(s)$ tends to be infinite, the grid-side current can track i_2^* and is almost independent of the grid voltage. That is to say, the gain of $G_R(s)$ at the grid background harmonics is required to be large enough.

Therefore, this paper adopts resonance controller to suppress the current harmonics caused by grid background harmonics and the ideal resonance controller is given as (3):

$$G_R(s) = \frac{k_{ir}s}{s^2 + w_h^2} \tag{3}$$

where k_{ir} is the coefficient of the controller's integral and w_h is the resonant frequency.

The gain at grid background harmonic frequency is

$$\left|G_R(s)\right|_{s=jw_h} = \sqrt{\left(\frac{k_{ir}w_h}{-\left(w_h\right)^2 + \left(w_h\right)^2} \right)^2} \rightarrow \infty \tag{4}$$

It is clear from (4) that the gain of $G_R(s)$ at grid background harmonic frequency is infinite, so it can suppress the grid-side current harmonics.

However, in practice, the ideal resonant controller is challenging to implement in digital systems due to the accuracy of the components and discrete control. Furthermore, when the frequency of the grid fluctuates, the harmonic mitigation capability of the controller significantly decreases because the gain in the ideal resonance controller sharply declines

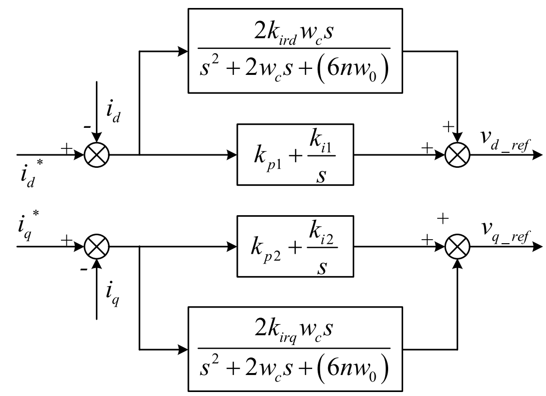

Fig. 3 Block diagram of proportional integral resonance control

outside the resonance frequency. Therefore, a quasi-resonant controller is expressed in (5):

$$G_R(s) = \frac{k_{ir}s}{s^2 + 2w_c s + w_h^2} \tag{5}$$

where w_c is the cutoff frequency and its value ranges from 5 ~ 20 rad/s.

The gain at the harmonic frequency is

$$\left|G_R(s)\right|_{s=jw_h} = \sqrt{\left(\frac{k_{ir} * jw_h}{-\left(w_h\right)^2 + 2w_c * \left(jw_h\right) + \left(w_h\right)^2} \right)^2} = \frac{k_{ir}}{2w_c} \tag{6}$$

According to (6), the greater k_{ir} is, the higher the gain at the resonant frequency is. However, if k_{ir} is too great, the stability and convergence of the system will be affected. A too small w_c can reduce the bandwidth of the controller. Therefore, $w_c = 5$ and $k_{ir} = 800$, 400 are selected as the cutoff frequency and integral coefficient of resonant controller to suppress the 5th, 7th and 11th harmonics.

Both proportional resonant (PR) regulator and proportional integrator (PI) regulator can track the output current reference accurately. However, PR controller regulates the output current in $\alpha\beta$ stationary frame. When the grid current contains 5th, 7th, 11th, and 13th harmonics, four resonant controllers need to be designed, which increases complexity of the controller design and degrades system stability. PI controller regulates the output current in dq synchronous frame and harmonics with the same orders, which can be suppressed by two resonant controllers with resonant frequencies ($6w_0$ and $12w_0$) [30], thus reducing complexity of the control system. Hence, this paper adopts PI + HC to control the grid-side current.

The block diagram of the proportional integral and quasi-resonant controller is shown in Fig. 3, where v_{d_ref} and v_{q_ref} are the outputs of the controller and the controller is expressed in (7):

$$G_c(s) = k_p + \frac{k_i}{s} + \frac{2k_{ir}w_c s}{s^2 + 2w_c s + (6nw_0)} \tag{7}$$

2.2 Stability Analysis of the System

Ignoring the effects of component-derived resistors, the open loop transfer function of the control system is expressed as (8):

$$T_i = G_c(s)G_d(s)k_{PWM}G_1(s)G_2(s) \tag{8}$$

The stability analysis is carried out using the Logarithmic frequency stability criterion. The Bode diagram is drawn based on the open loop transfer function of the control system and parameters in Table 1. In the open-loop Bode diagram, only the frequency ranges with magnitudes above 0 dB are considered. For the phase plot in these ranges, a ±(2 k + 1)π crossing in the direction of phase rising is defined as a positive crossing, while a crossing in the direction of phase falling is defined as a negative crossing. N + and N– denote the numbers of the positive and negative crossings, respectively. According to the Logarithmic frequency stability criterion, the number of the open-loop unstable poles P must meet P = 2(N + – N–) to ensure system stability. As can be seen from (5), (7), (8) and (9), P = 0, so N + – N– = 0 is required for the control systems.

Figure 4 is the open-loop Bode diagrams of GCF with different delays.

It can be seen that with $T_d = 0$, there is only a negative crossing, i.e. N– = 1, so the control system is unstable. By increasing time delays, the control system becomes stable.

Table 1 Parameters of LCL grid-connected inverter

Parameter	Symbol	Value
Power rating	P	1.0 kW
DC source	V_{dc}	140 V
Grid voltage	v_g	$40 \times \sqrt{2}$ V
Inverter-side inductor	L_1	1.5 mH
Grid-side inductor	L_2	1.5 mH
Filter capacitor	C	10 µF
Resonant angular frequency	ω_{res}	11555 rad/s
Switching frequency	f_{sw}	15 kHz
Switching period	T_{sw}	1/15 ms
Sampling frequency	f_s	15 kHz

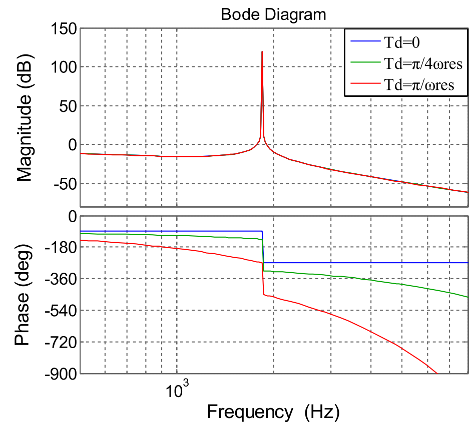

Fig. 4 Bode diagrams of GCF loop gain with different delays (PI + HC)

For instance, when $T_d = \pi/\omega_{res}$, N + = N– = 0, the system keeps stable. Therefore, increasing time delays to a certain extent can improve system stability [31]. However, making the system stable only by adjusting time delay has certain limitations in engineering applications. So an improved active damping is needed.

3 Grid-Side Current Feedback Control System Based on Improved HPF

Grid background harmonics can cause current distortion and affect the quality of the output power of the grid-connected LCL-filtered inverter. The GCF can control the grid-side current directly and mitigate harmonics of the grid-side current. Moreover, it does not require extra high-accuracy sensors to obtain harmonic information of the grid-side current. However, as discussed in Section II, GCF control system is unstable so it requires an active damping strategy. In this paper, improved HPF active damping with delay feedback is used by employing output current. Figure 5 shows the equivalent control block diagram of the improved HPF in the s-domain.

Where $W(s) = \frac{1}{1+e^{-\lambda s T_s}} G_H(s)$, $G_H(s) = -\frac{k_H}{s+w_d}$.

Figure 5 can be equivalently transformed into Fig. 6: the output of $W(s)$ is moved to the output of $1/(sL_1)$, and the

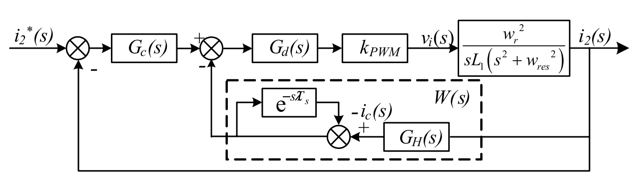

Fig. 5 Active damping control diagram of GCF based on improved HPF

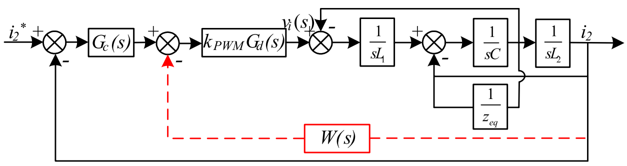

Fig. 6 Active damping control diagram of GCF based on improved HPF

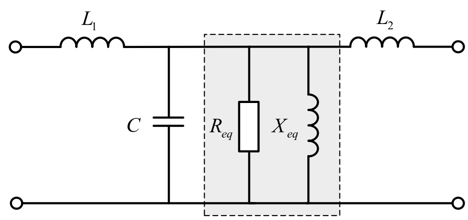

Fig. 7 The circuit of equivalent virtual impedance

input of $W(s)$ is moved to the output of $1/(sC)$. The equivalent control block diagram is shown in Fig. 6, where the active damping strategy can be regarded as virtual impedance in reverse parallel with the capacitor C.

z_{eq} is obtained as (9):

$$z_{eq} = \frac{sL_1L_2}{k_{PWM}G_d(s)W(s)} \tag{9}$$

By substituting $W(s)$ and $G_H(s)$ into (8), z_{eq} can be obtained as (10):

$$z_{eq}(s,\lambda) = \frac{-s\left(s+w_d\right)L_1L_2\left(e^{1.5sT_s}+e^{(1.5-\lambda)sT_s}\right)}{k_{PWM}k_H} \tag{10}$$

Substituting $s=jw$ into (10) obtains the equivalent virtual resistance and inductance in parallel, as shown in Fig. 7, where R_{eq} and X_{eq} are expressed in (11):

$$\begin{cases} R_{eq}(w,\lambda) = \dfrac{wL_1\left(L_2+L_g\right)\left(w^2+w_d^2\right)g(w,\lambda)}{k_{PWM}k_Hg_R(w,\lambda)} \\ X_{eq}(w,\lambda) = \dfrac{wL_1\left(L_2+L_g\right)\left(w^2+w_d^2\right)g(w,\lambda)}{k_{PWM}k_Hg_X(w,\lambda)} \end{cases} \tag{11}$$

$g(w,\lambda)$,$g_R(w,\lambda)$ and $g_X(w,\lambda)$ in (11) are expressed in (12):

$$\begin{cases} g(w,\lambda) = \cos\left(\dfrac{\lambda}{2}wT_s\right) \\ g_R(w,\lambda) = \sqrt{w^2+w_d^2}\sin\left(\dfrac{3-\lambda}{2}wT_s+\theta\right) \\ g_X(w,\lambda) = -\sqrt{w^2+w_d^2}\cos\left(\dfrac{3-\lambda}{2}wT_s+\theta\right) \end{cases} \tag{12}$$

Table 2 Equivalent impedance analysis when λ = 1

Equivalent impedance	$(0, f_{1X})$	(f_{1X}, f_{1R})	$(f_{1R}, f_{s/2})$
Req	+	–	–
X_{eq}	–	+	–

Table 3 Equivalent impedance analysis when λ = 2

Equivalent impedance	$(0, f_{s/4})$	$(f_{s/4}, f_{2X})$	$(f_{2X}, f_{s/2})$
Req	+	–	–
X_{eq}	–	+	–

Where "+, –" represent positive and negative characteristics of R_{eq} and X_{eq}

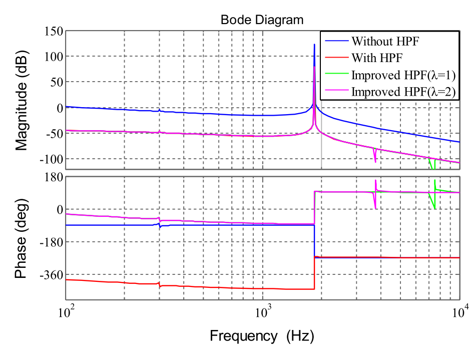

Fig. 8 Bode diagrams of control system using HPF with different delay feedbacks

Equations (11) and (12) show that the equivalent virtual resistance is not always positive in the effective damping range $(0, f_s/4)$ when λ = 0 or λ ≥ 3. Therefore, λ can only take 1 or 2 as value.

Tables 2 and 3 show the equivalent impedance at different ranges of frequency with λ = 1 and λ = 2, respectively. It can be derived that the effective damping region of the system is $(0, f_{1R})$ for λ = 1, while λ = 2 is $(0, f_s/4)$, where $f_{1R} \in (f_s/4, f_s/2)$.

Figure 8 shows Bode diagram of the control system using HPF and the improved HPF with different delay feedbacks. The system becomes stable at f_{res} with HPF regardless of the value of λ. It is worth noting that the magnitude and phase exhibit new peaks at 3800 Hz and 7800 Hz with λ = 1 and λ = 2, respectively. However, the stability of system cannot be affected by the new peak of negative magnitude. Finally, an improved HPF with unit delay feedback ($\lambda=1$) is chosen owing to its larger damping region than HPF and improved HPF with $\lambda=2$.

4 Simulation and Experimental Results

Simulations and experiments were conducted to assess effectiveness and correctness of the proposed method. The parameters of the grid-connected LCL-filtered inverter control system were shown in Table 1.

4.1 Simulation Results

The GCF control system using the improved HPF was built in MATLAB/PLEC with $T_d=1.5\ T_s$ and 5% of the seventh harmonic to simulate the grid background harmonics. The current reference of the grid is 5 A and the improved HPF is employed at 0.01 s.

Figure 9 showed the dynamic process of employing HPF. The grid-side current feedback control system was unstable without HPF. By introducing the improved HPF at 0.01 s, the inverter-side current and grid-side current reached their reference values after a transient transition of 0.01 s, demonstrating that the system became stable.

According to previous works [7–10], grid background harmonics caused a distortion in the grid-side current and degraded quality of the output power of the LCL-filtered inverter. This paper thus controlled the grid-side current directly by adopting PI + HC to mitigate the seventh harmonic. Figure 10 illustrates waveforms of the inverter-side current and grid-side current with HC employed at 0.08 s.

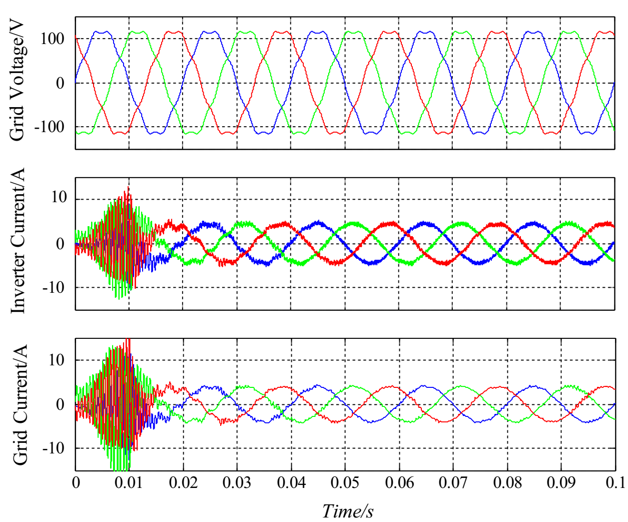

Fig. 9 Waveforms of inverter-side current and grid-side current based on the improved HPF

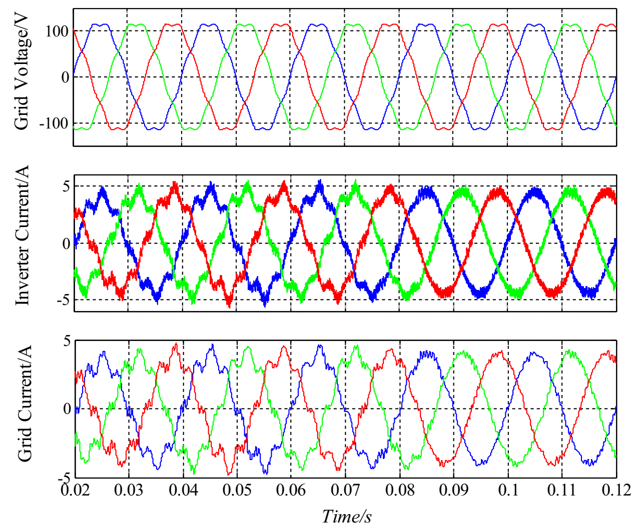

Fig. 10 Waveforms of inverter-side current and grid-side current before and after HC

The control system is controlled by PI before 0.08 s and the output current tracked the reference value of 5 A. However, the PI controller could not reduce the grid-side current harmonics caused by the grid background harmonics, which degrades the quality of the output power of the inverter. By introducing HC at 0.08 s, as displayed in Fig. 10, the seventh harmonic of the grid-side current reduces after about half a period of the transient process, which showed the effectiveness of the resonance controller.

To further illustrate the effectiveness of the PI + HC, the total harmonic distortion (THD) of the grid-side current i_2 was compared in Figs. 11 and 12. Figures 11 and 12 show

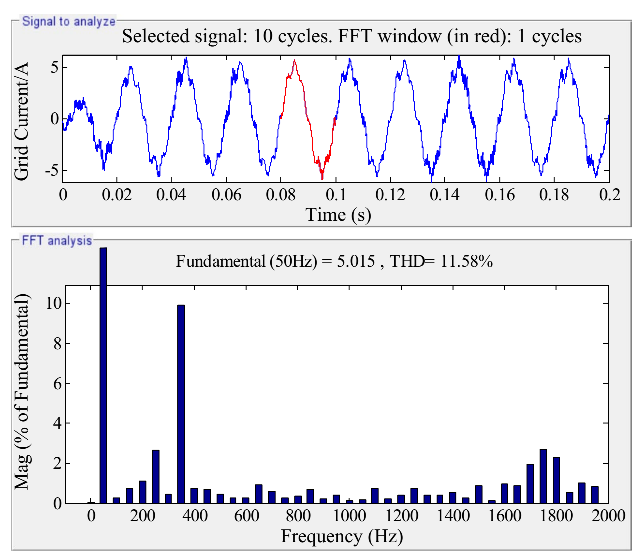

Fig. 11 The waveform and harmonic spectrum of grid-side current without the proposed strategy

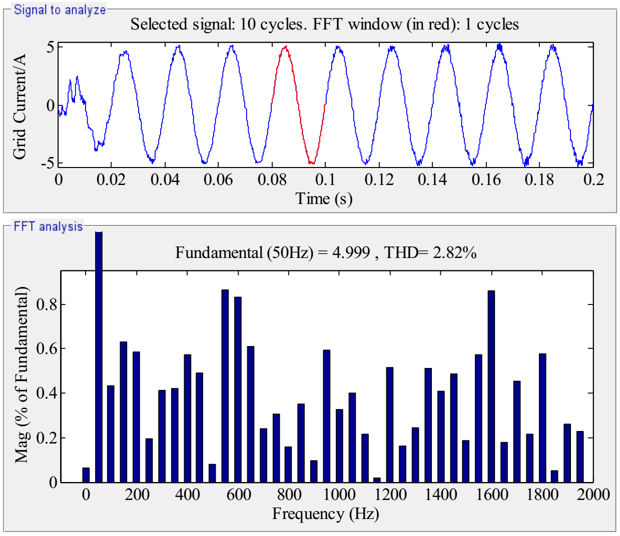

Fig. 12 The waveform and harmonic spectrum of grid-side current with the proposed strategy

the waveform and harmonic spectrum of i_2 with the PI controller and PI + HC, respectively.

As shown in Fig. 11, the grid-side current i_2 presents significant distortion, with a THD of 11.58%, mainly centering on 350 Hz. The THD does not satisfy grid standards such as the IEEE Std 929-2000.

By contrast, the grid-side current is effectively improved by HC and the harmonics at 350 Hz significantly reduces in Fig. 12. The THD is 2.82%, which meets the IEEE Std 929-2000, whereby the THD of the current should be < 5%.

Figure 13 shows the dynamic process of the system when the grid-side current i_2 increases from 5 to 10 A with PI + HC. The grid current tracks the changed value in less than a period and reduces the grid-side current harmonics, which indicates that the control system could operate stably and perform well during the dynamic process.

To further illustrate the stability of the control system, a total of 5% of the 5th, 7th, and 11th harmonics are injected. The simulation results are shown in Fig. 14.

4.2 Experimental Results

To further test the effectiveness of the proposed strategy, experiments were carried out on the dSPACE DS1104 platform and its output signals were transformed to the IGBT on the inverter's bridge. The non-ideal grid and DC power supply were implemented using Chroma 61511 and HAP60-600, respectively. LV28-P and LEM LT208-S7/SP1 were employed to sense the PCC voltage and the grid-side current, respectively. The switching devices were Infineon K75T60 and series IGBT. The input DC voltage and Root-Mean-Square (RMS) value of grid voltage were 150 V and 40 V, respectively. The other parameters were shown in Table 1.

Figure 15 shows waveforms of the grid voltage v_g and i_2 with seventh harmonic during the dynamic process. Before the improved HPF was employed, the control system was unstable and featured significant resonance in the grid-side current i_2, which rendered the PI + HC to be invalid. When the improved HPF is used, resonance in the grid-side current i_2 reduces, which shows the effectiveness of the improved HPF.

Under the premise of ensuring the stability of the GCF system, PI + HC were employed to mitigate the harmonics of

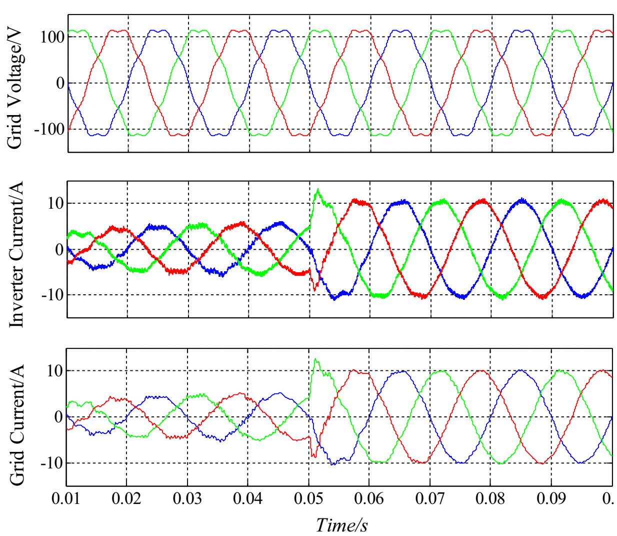

Fig. 13 Transient waveforms of inverter current i_1 and grid current i_2 with the proposed strategy

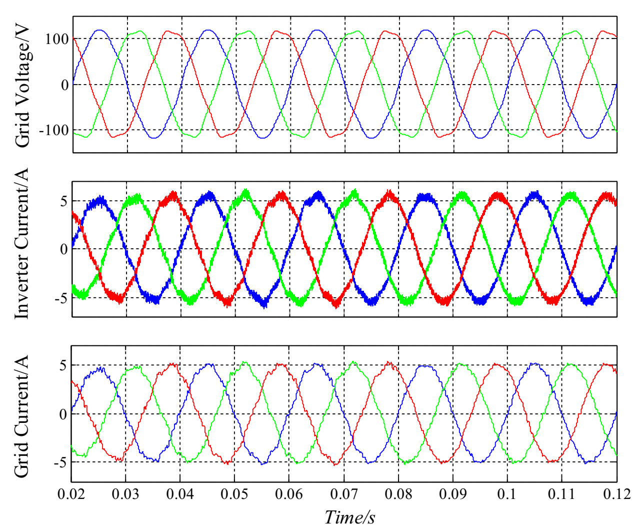

Fig. 14 Waveforms of inverter-side current and grid-side current before and after HC

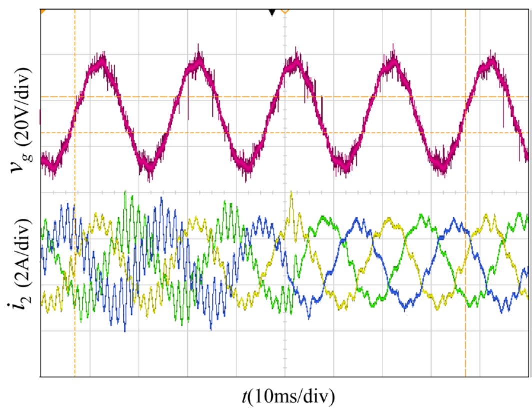

Fig. 15 Waveforms of i_2 with seventh harmonic before and after HPF

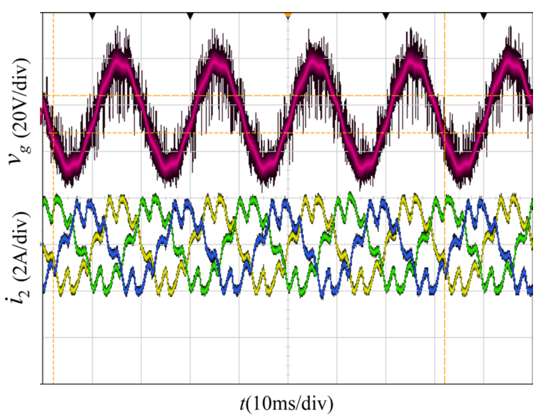

Fig. 16 Waveforms of i_2 with seventh harmonic using PI

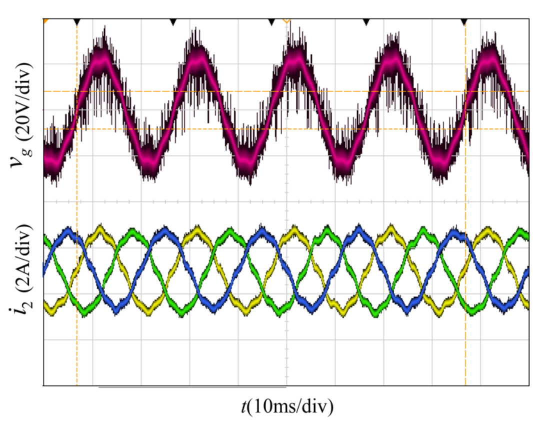

Fig. 17 Waveforms of i_2 with seventh harmonic using PI + HC

the grid-side current i_2. Figures 16 and 17 show waveforms of the grid-side current i_2 with PI controller and PI + HC, respectively.

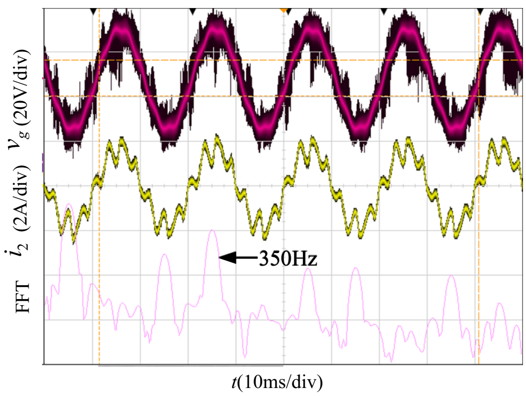

Fig. 18 Waveforms and spectrum of i_2 with seventh harmonic using PI

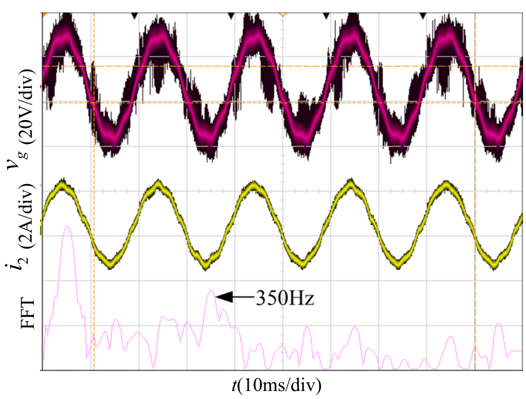

Fig. 19 Waveforms and spectrum analysis of i_2 with seventh harmonic using PI + HC

Figure 16 shows that when the grid voltage contains the seventh harmonic, it distorts the grid-side current and affects the quality of the output power of the LCL-filtered inverter.

Comparatively, Fig. 17 shows the grid-side current i_2 with PI + HC. The added resonant controller effectively reduces distortion in the grid-side current caused by the grid harmonic, thus demonstrating the effectiveness of the HC resonant control design.

To further confirm the reduction in harmonics using HC, a spectrum analysis of the grid-side current i_2 is carried out, shown in Fig. 18. The single-phase waveforms and spectrum analysis of grid-side current i_2 before HC were employed and Fig. 18 shows the waveforms and spectrum analysis of i_2 using HC. As shown in Fig. 18, the distortion in the grid-side current is severe and large volume of harmonics is observed at 350 Hz.

By contrast, Fig. 19 shows the single-phase waveforms of the grid-side current i_2 using HC, where the harmonics at 350 Hz significantly reduces. This verifies the correctness of parameters of the HC.

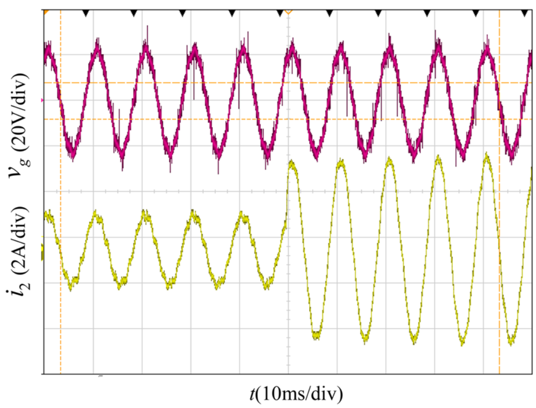

Fig. 20 Transient waveform of i_2 with seventh harmonic after HC

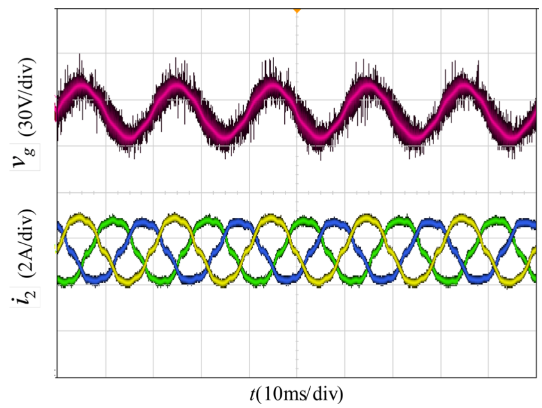

Fig. 22 Waveforms of grid-side current after HC with 5th, 7th and 11th harmonics injected

Figure 20 shows the dynamic response of the reference value of the grid-side current from 1 to 3 A. When the reference value changes, the grid-side current i_2 quickly tracks the given value and runs stably, which shows that the control system manifests perfect dynamic performance and stability.

Figures 21 and 22 show the waveform of grid-side current before and after HC (with a total of 5% of the 5th, 7thand 11th harmonics injected), respectively. It can be seen that the proposed method can suppress the distortion caused by grid background harmonics and maintain stability when other orders harmonics are injected.

5 Conclusions

This paper proposed a method for mitigating distortion of grid-side current for the grid-connected LCL-filtered inverter. The proposed strategy could reduce cost and system complexity by controlling the grid-side current directly. The PI + HC control algorithm reduced the distortion in grid-side current caused by grid background harmonics. To ensure the stability of the system and effectiveness of the proposed algorithm, an improved HPF with active damping based on unit delay feedback was used. Simulation and experimental results show that the control strategy can improve the quality of grid-side current under non-ideal grid condition, thereby guaranteeing the output power quality of grid-connected inverter.

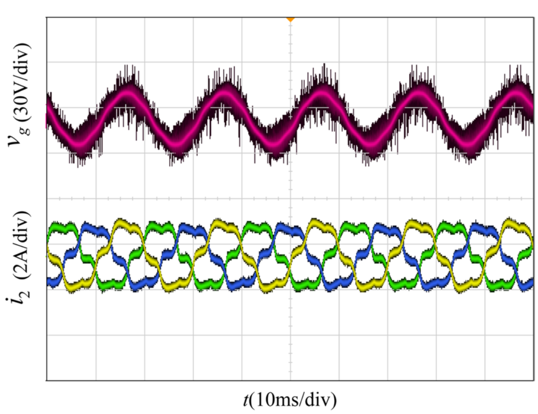

Fig. 21 Waveforms of grid-side current before HC with 5th, 7th and 11th harmonics injected

References

1. Blaabjerg F, Teodorescu R, Liserre M, Timbus AV (2006) Overview of control and grid synchronization for distributed power generation systems. IEEE Trans Industr Electron 53(5):1398–1409
2. Xu JM, Xie SJ, Zhang B (2015) Overview of current control techniques for grid-connected inverters with LCL filters in distributed power generation systems. Proc CSEE 35(16):4153–4166
3. Xu JM, Ji L, Ge XW, Xie SJ (2016) LCL-filter optimization design with consideration of inverter-side current feedback control impacts. Proc CSEE 36(17):4656–4664
4. Lu MH, Al-Durra A, Muyeen SM, Leng SY, Loh PC, Blaabjerg F (2018) Benchmarking of stability and robustness against grid impedance variation for LCL filtered grid-interfacing inverters'. IEEE Trans Power Electron 33(10):9033–9046
5. Beres RN, Wang XF, Blaabjerg F, Liserre M, Bak CL (2016) A review of passive power filters for three-phase grid connected voltage-source converters. IEEE J Emerg Select Topics Power Electron 4(1):54–69
6. Peña-Alzola R, Liserre M, Blaabjerg F, Sebastián R, Dannehl J, Fuchs FW (2013) Analysis of the passive damping losses in LCL-filter-based grid converters. IEEE Trans Power Electron 28(6):2642–2646
7. Dannehl J, Liserre M, Fuchs FW (2011) Filter-based active damping of voltage source converters with filter. IEEE Trans Industr Electron 58(8):3623–3633
8. Tang Y, Loh PC, Wang P, Choo FH, Gao F, Blaabjerg F (2012) Generalized design of high performance shunt active power

filter with output LCL filter. IEEE Trans Industr Electron 59(3):1443–1452
9. He J, Li Y (2012) Generalized closed-loop control schemes with embedded virtual impedances for voltage source converters with LC or LCL filters. IEEE Trans Power Electron 27(4):1850–1861
10. Pan DH, Ruan XB, Wang XH, Yu H, Xing ZW (2017) Analysis and design of current control schemes for LCL-type grid-connected inverter based on a general mathematical model. IEEE Trans Power Electron 32(6):4395–4410
11. Liu BY, Wei QK, Zou CY, Duan SX (2018) Stability analysis of LCL-type grid-connected inverter under single-loop inverter-side current control with capacitor voltage feedforward. IEEE Trans Industr Inf 14(2):691–702
12. Pena-Alzola R, Liserre M, Blaabjerg F, Ordonez M, Kerekes T (2014) A self-commissioning notch filter for active damping in a three-phase LCL-filter-based grid-tie converter. IEEE Trans Power Electron 29(12):6754–6761
13. Saleem M, Choi K-Y, Kim R-Y (2019) Resonance damping for an LCL filter type grid-connected inverter with active disturbance rejection control under grid impedance uncertainty. Electr Power Energy Syst 109:444–454
14. Xin Z, Loh PC, Wang XF, Blaabjerg F, Tang Y (2016) Highly accurate derivatives for LCL filtered grid converter with capacitor voltage active damping. IEEE Trans Power Electron 31(5):3612–3625
15. Li XQ, Wu XJ, Geng YW, Yuan XB, Xia CY (2015) Wide damping region for LCL-type grid-connected inverter with an improved capacitor-current-feedback method. IEEE Trans Power Electron 30(9):5247–5258
16. Pan DH, Ruan XB, Wang XH, Bao CL, Li WW (2013) A Capacitor-current real-time feedback active damping method for improving robustness of the LCL-type grid-connected inverter. Proc CSEE 33(18):1–10
17. Enrique RD, Freijedo FD, Juan V, Guerrero JM (2019) Analysis and comparison of notch filter and capacitor voltage feedforward active damping techniques for LCL grid-connected converters. IEEE Trans Power Electron 34(4):3958–3972
18. Qian Q, Xie SJ, Huang LL, Xu JM, Zhang Z, Zhang B (2017) Harmonic mitigateion and stability enhancement for parallel multiple grid-connected inverters based on passive inverter output impedance'. IEEE Trans Industr Electron 64(9):7587–7598
19. Mohamed ARI (2011) Mitigation of dynamic, unbalanced, and harmonic voltage disturbances using grid-connected inverters with LCL filter'. IEEE Trans Industr Electron 58(9):3914–3924
20. Xin Z, Mattavelli P, Yao WL, Yang YH, Blaabjerg F (2018) Mitigation of grid-side current distortion for LCL filtered voltage source inverter with inverter side current feedback control. IEEE Trans Power Electron 33(7):6248–6261
21. Twining E, Holmes DG (2003) Grid current regulation of a three-phase voltage source inverter with an LCL input filter. IEEE Trans Power Electron 18(3):888–895
22. Fei L, Yan Z, Shanxu D, Jinjun Y, Bangyin L, Fangrui L (2009) Parameter design of a two-current-loop controller used in a grid-connected inverter system with LCL filter. IEEE Trans Industr Electron 56(11):4483–4491
23. Jia YQ, Zhao J, Fu X (2013) Direct grid current control of LCL-filtered grid-connected inverter mitigating grid voltage disturbance. IEEE Trans Power Electron 29(3):1532–1541
24. Liu Y, Wu W, He YB, Lin Z (2016) An efficient and robust hybrid Damper for LCL- or LLCL-based grid-tied inverter with strong grid-side harmonic voltage effect rejection. IEEE Trans Ind Electron 63(2):1–10
25. Wang XH, Ruan XB, Liu SW (2012) Control strategy for grid-connected inverter to suppress current distortion effected by background harmonics in grid voltage. Proc CSEE 31(6):7–14
26. Wu XJ, Li XQ, Yuan XB, Geng YW (2015) Grid harmonics suppression scheme forLCL-type grid-connected inverters based on output admittance revision. IEEE Trans Sustain Energy 6(2):411–421
27. Xu JM, Xie SJ, Qian Q, Zhang B (2017) Adaptive feedforward algorithm without grid Iimpedance estimation for inverters to suppress grid current instabilities and harmonics due to grid impedance and grid voltage distortion. IEEE Trans Ind Electron 64(9):7574–7586
28. Diego PE, Jesus DG, Alejandro GY, Oscar L (2018) Generalized multi-frequency current controller for grid-connected converters with LCL filter. IEEE Trans Ind Appl 54:4537–4553
29. Devaraddi SM, Sandhya P (2017) Harmonie mitigation in multi feeders by using MC-UPQC system with the predictive ANN & SVM[C]//2017 International Conference On Smart Technologies For Smart Nation (Smart Tech Con). IEEE, 2017
30. Zhang HY, Xu HP, Fang C, Xiong C (2017) Torque ripple mitigateion method of direct-drive permanent magnet synchronous based on proportional-integral and quasi resonant controller. Trans China Electrotech Soc 32(19):41–51
31. Wang JG, Yan JD, Jiang L, Zou JY (2015) Delay-dependent stability of single-loop controlled grid-connected inverters with LCL filters. IEEE Trans Power Electron 31(1):1–14

Ye Zhang (S') was born in Hebei, China, in November 1986. She received the B.S. degree in electrical engineering from China University of Mining and Technology, China in 2011, the M.S. degree from Tianjin University, China, in 2014. Since then, she has been a teacher in Taiyuan Institute of Technology and currently she is also a Ph.D. candidate in the Power Engineering, Taiyuan University of Technology. Her research interests include power quality analysis and control of power converters for renewable energy systems.

Muqin Tian was born in Shanxi, China, in June 1962. She received the B.S. degree from Dalian Railroad Institute, China, in 1987, the M.S. degree from Taiyuan University of Technology, China, in1990, and the Ph.D. degree from Taiyuan University of Technology, China, in 2006. Her main interest is state monitoring and early warning of large mechanical equipment and intelligent control. Currently, she is director of the Department of Electrical Engineering at Taiyuan University of Technology. Currently, she is director of the Department of Electrical Engineering at Taiyuan University of Technology.

Jiancheng Song (M'13) was born in Shanxi, China, in 1957. He received the B.Sc. degree from Taiyuan University of Technology, China, in 1982, the M.Sc. degree from Newcastle University, England, in 1987, respectively and the Ph.D. degree from Xi'an Jiaotong University, China, in 1999. Currently, he is a professor of the College of Electrical and Power Engineering at Taiyuan University of Technology. He has experience in the field of condition assessment, remaining life assessment and intellectual automation technology. He has performed a number of electrical failure investigations about coal mine. He has presented a number of technical and scientific papers at international conferences and seminars.

Xiaoyu Zhang was born in Henan, China, in May 1990. He received the B.S. degree in coal mining engineering from Taiyuan University of Technology, China in 2014, Currently, he is a Ph.D. candidate in the college of coal mining engineering, Taiyuan University of Technology. His research interests include electrochemistry modification and methane extraction.